

# Analytical solutions for the Bohr Hamiltonian with the Woods–Saxon potential

M Çapak<sup>1</sup>, D Petrellis<sup>2</sup>, B Gönül<sup>1</sup> and Dennis Bonatsos<sup>3</sup>

<sup>1</sup> Department of Engineering Physics, University of Gaziantep, 27310 Gaziantep, Turkey

<sup>2</sup> Department of Physics, University of Istanbul, 34134 Vezneciler, Istanbul, Turkey

<sup>3</sup> Institute of Nuclear and Particle Physics, National Centre for Scientific Research “Demokritos”, GR-15310 Aghia Paraskevi, Attiki, Greece

E-mail: gonul@gantep.edu.tr

## Abstract.

Approximate analytical solutions in closed form are obtained for the 5-dimensional Bohr Hamiltonian with the Woods–Saxon potential, taking advantage of the Pekeris approximation and the exactly soluble one-dimensional extended Woods–Saxon potential with a dip near its surface. Comparison to the data for several  $\gamma$ -unstable and prolate deformed nuclei indicates that the potential can describe well the ground state and  $\gamma_1$  bands of many prolate deformed nuclei corresponding to large enough “well size” and diffuseness, while it fails in describing the  $\beta_1$  bands, due to its lack of a hard core, as well as in describing  $\gamma$ -unstable nuclei, because of the small “well size” and diffuseness they exhibit.

PACS numbers: 21.60.Ev, 21.60.Fw, 21.10.Re

*Keywords:* Bohr Hamiltonian, Woods-Saxon potential, Pekeris approximation

## 1. Introduction

The advent of critical point symmetries [1, 2], related to shape/phase transitions in nuclear structure [3, 4], has stirred interest in analytical solutions (exact or approximate) [5] of the Bohr Hamiltonian [6]. In addition to the infinite well potential, used in the critical point symmetries E(5) [1] and X(5) [2], related to the transition from spherical to  $\gamma$ -unstable (soft with respect to triaxiality) [7] and to prolate deformed [8] nuclei respectively, solutions involving the Davidson [9, 10, 11, 12, 13], Kratzer [14, 15, 16, 17], and Morse [18, 19, 20] potentials (shown in figure 1) have been given. When applied to the bulk of nuclei for which energy spectra and B(E2) transition rates are experimentally known [21], all these potentials provide good and quite similar results [12, 13, 15, 16, 17, 19, 20], despite having quite different shapes.

The question arises if the success of the above mentioned potentials is due to the form of the Bohr Hamiltonian alone, or if there are potentials which, when plugged into the Bohr Hamiltonian, will not be able to provide satisfactory results for nuclear data.

In this work we consider the Woods–Saxon potential [22], which has been extensively used in nuclear physics in a different context, namely as a single-particle potential [23]. The potential, shown in figure 1(c), reads

$$U_{WS}(\beta) = -\frac{U_0}{e^{2a(\beta-\beta_0)} + 1}, \quad (1)$$

where  $U_0$ ,  $a$  and  $\beta_0$  are non-negative free parameters. This study is motivated by several reasons.

1) For  $a \rightarrow \infty$  the WS potential reduces to a finite square well potential, which has also been used in relation to critical point symmetries [24, 25], in addition to the infinite well potential [1, 2].

2) In contrast to the Davidson [9], Kratzer [14], and Morse [18] potentials, which possess a hard core, the WS potential does not have a hard core. We will find out the consequences of this difference.

3) The Woods–Saxon potential is also interesting from the mathematical point of view, since it has no closed analytical solution for the spectrum, even in one dimension and for vanishing angular momentum [26, 27]. Only an analytical wavefunction is known in one dimension and for vanishing angular momentum [27].

First we manage to produce approximate solutions in closed form for the WS potential with a centrifugal barrier, exploiting its resemblance (after applying the Pekeris approximation [28] to it) to a modified spherically symmetric WS potential [29] known to possess exact analytical solutions [26]. Taking advantage of these solutions within the framework of the Bohr Hamiltonian we subsequently fit several  $\gamma$ -unstable and prolate deformed nuclei, pointing out the successes, but also the failures of the WS potential.

Numerical calculations involving generalized forms of the Bohr Hamiltonian have a long history.

1) Extensive early numerical calculations for vibrating axially symmetric deformed nuclei have been performed in the framework of the Rotation Vibration Model [30, 31].

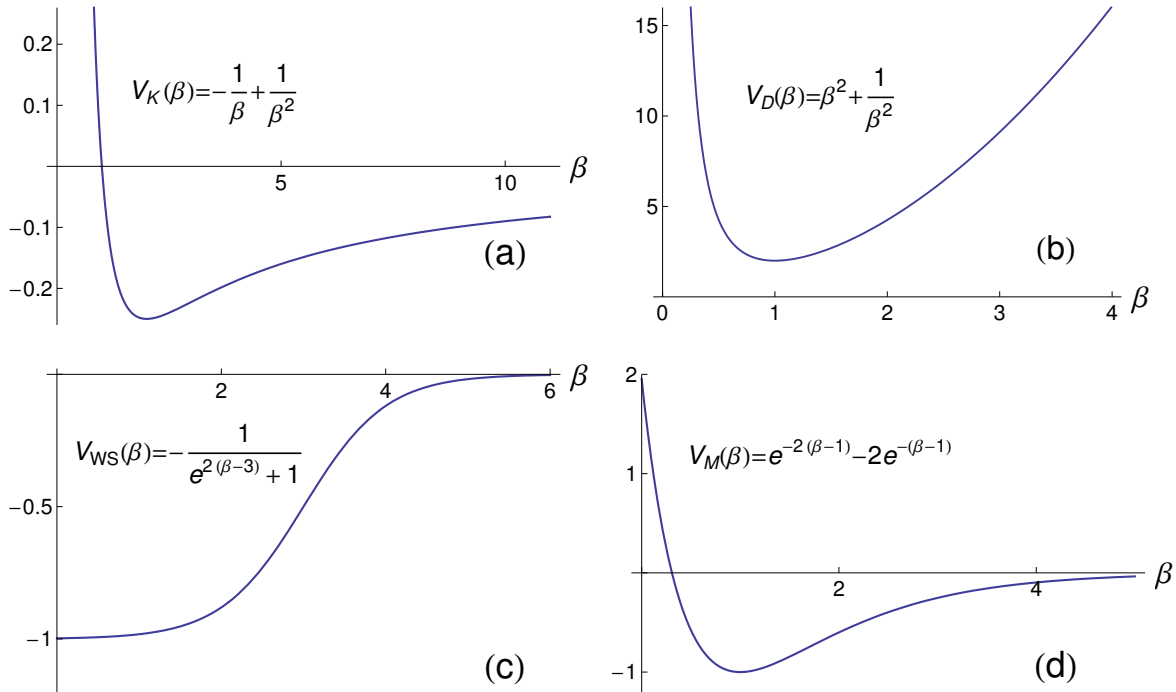


**Figure 1.** (Color online) The Kratzer [14] (a), Davidson [9] (b), Woods–Saxon [22] (c) and Morse [18] (d) potentials, for special values of their free parameters, used for simplicity. All quantities shown are dimensionless.

2) Numerical solutions have subsequently been provided using a general form for the potential energy [32, 33], giving emphasis on the restrictions imposed on the form of the potentials by symmetry constraints.

3) Extensive numerical results using a general collective model employing general forms of both the kinetic energy and the potential energy have been obtained initially [34] by using a basis provided by Hecht [35], and subsequently [36, 37] by exploiting the basis of a 5-dimensional (5D) harmonic oscillator [38, 39].

4) The recent clarification [40] of the group theoretical structure of the Davidson potential, when used in the framework of the Bohr Hamiltonian, led to the development of the Algebraic Collective Model [41, 42, 43, 44], which allows the efficient numerical calculation of spectra and transition probabilities of nuclei of any shape.

In addition to the  $\gamma$ -unstable and the prolate deformed nuclei, the description of triaxial nuclei within the framework of the Bohr Hamiltonian was very early attempted [45, 46] and is still attracting considerable attention [25, 47, 48, 49, 50].

On the other hand, studies on the microscopic foundation of the Bohr Hamiltonian have a long history, some early efforts reported in [51, 52, 53]. Efforts towards the derivation of the Bohr collective Hamiltonian through the adiabatic approximation of the time-dependent Hartree-Fock-Bogolyubov theory (the ATDHFB method), as well as through the generator coordinate method with the Gaussian overlap approximation (the GCM+GOA method) have been reviewed in [54]. Recently, the derivation of the

parameters to be used in a 5D Hamiltonian for quadrupole vibrational and rotational degrees of freedom from Relativistic Mean Field (RMF) calculations [55, 56, 57, 58] is acquiring momentum.

## 2. Modified Woods–Saxon potential with a centrifugal barrier

### 2.1. Pekeris approximation for the centrifugal barrier

The Pekeris approximation [28] is a well known method for finding approximate analytical solutions for potentials involving exponentials. It has been introduced in relation to the Morse potential [18] with a centrifugal barrier in studies of rotational-vibrational spectra of diatomic molecules [28]. The basic idea of the Pekeris approximation is to rewrite approximately the centrifugal term using exponentials resembling the ones appearing in the rest of the potential, with the aim to be able to “absorb” the centrifugal term into the potential.

This approximation has been used in relation with the Morse potential in diatomic molecules [28, 59], as well as with the pseudo-centrifugal term for Dirac particles within Morse potentials [60]. Furthermore, a supersymmetric improvement of the Pekeris approximation in the case of the Morse potential has been worked out [61]. Numerical results reported in these papers indicate that the approximation works well, especially for relatively low-lying vibrational and rotational states (see in particular the detailed results reported in [61]).

The Pekeris approximation has further been used in relation to various exponential-type potentials [62], to the Wei Hua oscillator [63], to the Rosen–Morse and Manning–Rosen potentials [64], as well as with the pseudo-centrifugal term for Dirac particles within Rosen–Morse potentials [65]. In these cases, various functions appear in the original potentials, as well as in the Pekeris approximation terms.

The spherically symmetric Woods-Saxon potential in three-dimensions with a centrifugal barrier reads

$$U(\beta) = U_{WS}(\beta) + U_c(\beta) = -\frac{U_0}{e^{2a(\beta-\beta_0)} + 1} + \frac{l(l+1)}{\beta^2}, \quad (2)$$

where  $U_{WS}$  stands for the Woods-Saxon potential,  $U_c$  stands for the centrifugal term,  $l$  is the angular momentum, while  $U_0$ ,  $a$  and  $\beta_0$  are non-negative free parameters.

It is known [26] that this potential cannot be solved exactly. However, closed analytical solutions can be derived using the Pekeris approximation [28]. As it was mentioned above, the basic idea of the Pekeris approximation is to rewrite approximately the centrifugal term using exponentials resembling the ones appearing in the rest of the potential, with the aim to be able to “absorb” the centrifugal term into the potential.

In the present case we wish to write the centrifugal term in the approximate form

$$U_c(\beta) = \frac{l(l+1)}{\beta^2} \approx \delta \left[ C_0 + \frac{C_1}{e^{2a(\beta-\beta_0)} + 1} + \frac{C_2}{[e^{2a(\beta-\beta_0)} + 1]^2} \right]. \quad (3)$$

In order to use a more compact notation, we introduce the change of coordinates  $x = (\beta - \beta_0)/\beta_0$ . Then the exact centrifugal term takes the form

$$U_c(x) = \frac{\delta}{(1+x)^2}, \quad (4)$$

where

$$\delta = \frac{l(l+1)}{\beta_0^2}. \quad (5)$$

Expanding this function into binomial series one gets

$$U_c(x) = \delta(1 - 2x + 3x^2 - 4x^3 + \dots). \quad (6)$$

On the other hand, using the same notation, the approximate form of (3) becomes

$$U_c(x) \approx \delta \left[ C_0 + \frac{C_1}{e^{2a\beta_0 x} + 1} + \frac{C_2}{[e^{2a\beta_0 x} + 1]^2} \right]. \quad (7)$$

Expanding the exponentials in Taylor series we get

$$U_c(x) \approx \delta \left[ \left( C_0 + \frac{C_1}{2} + \frac{C_2}{4} \right) - \frac{\beta_0}{4a_0}(C_1 + C_2)x + \frac{\beta_0^2}{16a_0^2}C_2x^2 + \dots \right], \quad (8)$$

where

$$a_0 = \frac{1}{2a}. \quad (9)$$

Equating the coefficients of equal powers of  $x$  in (6) and (8) we get

$$C_0 = 1 - \frac{4a_0}{\beta_0} + \frac{12a_0^2}{\beta_0^2}, \quad C_1 = \frac{8a_0}{\beta_0} - \frac{48a_0^2}{\beta_0^2}, \quad C_2 = \frac{48a_0^2}{\beta_0^2}. \quad (10)$$

Using the approximate expression of (3) in (2), we obtain

$$U(\beta) \approx \delta C_0 - \frac{(U_0 - \delta C_1)}{e^{2a(\beta-\beta_0)} + 1} + \frac{\delta C_2}{[e^{2a(\beta-\beta_0)} + 1]^2}, \quad (11)$$

where indeed the centrifugal term has been “absorbed” in the potential.

The accuracy of approximating the potential of (2) by (11) will be discussed in detail in section 5, in relation to the parameter values occurring for the nuclei under consideration (see figs. 4, 5, 6 and relevant discussion in section 5).

## 2.2. Modified spherically symmetric Woods–Saxon potential

On the other hand, the modified spherically symmetric Woods–Saxon potential, which presents a dip near its surface [29], has the form

$$V(\beta) = -\frac{V_0}{e^{2a(\beta-\beta_0)} + 1} - \frac{W e^{2a(\beta-\beta_0)}}{[e^{2a(\beta-\beta_0)} + 1]^2}, \quad (12)$$

where  $V_0$ ,  $W$ ,  $a$  and  $\beta_0$  are non-negative free parameters. This potential, shown in figure 2, is known [26] to possess exact solutions of the one-dimensional Schrödinger equation in terms of Jacobi polynomials [66]

$$\Psi_n(\beta) \propto \left[ \frac{1}{e^{2a(\beta-\beta_0)} + 1} \right]^{b/2} \left[ 1 - \frac{1}{e^{2a(\beta-\beta_0)} + 1} \right]^{c/2} P_n^{(b,c)} \quad (13)$$

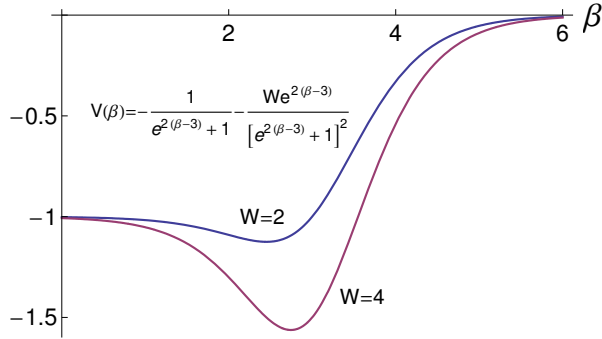


**Figure 2.** (Color online) The Woods–Saxon potential with a dip near its surface, given in (12), is shown for special values of its free parameters, used for simplicity. All quantities shown are dimensionless.

where

$$b = \frac{1}{2} \left( \tilde{\rho}_n + \frac{V_0}{a^2 \tilde{\rho}_n} \right), \quad c = \frac{1}{2} \left( \tilde{\rho}_n - \frac{V_0}{a^2 \tilde{\rho}_n} \right), \quad (14)$$

with

$$\tilde{\rho}_n = \sqrt{1 + \frac{W}{a^2}} - (2n + 1), \quad (15)$$

and the condition [66]

$$b, c > -1 \quad (16)$$

has to be fulfilled, implying the restriction

$$b + c > -2. \quad (17)$$

The strengths of the potential of (12) can be expressed in the form [26]

$$V_0 = a^2(b^2 - c^2) \geq 0, \quad (18)$$

$$W = a^2[(b + c)(b + c + 4n + 2) + 4n(n + 1)] \geq 0, \quad (19)$$

which imply stronger restrictions on  $b, c$ . Indeed, from (19) for  $n = 0$  one should have  $(b + c)(b + c + 2) \geq 0$ , which implies either  $b + c \leq -2$ , which is not allowed by (17), or

$$b + c \geq 0, \quad (20)$$

which is a stronger restriction. Higher values of  $n$  do not impose any further restrictions, since (19) leads to  $b + c \leq -2(n + 1)$ , which is not allowed by (17), or  $b + c \geq -2n$ , which is weaker than (17). It should be remembered that the quantity  $W$ , given in (19), cannot vanish, since in that case the potential of (12) would collapse to the usual Woods–Saxon potential, which is known to have no closed analytical solutions for its spectrum [26, 27].

The eigenvalues of the energy are known to be [26]

$$E_n = -\frac{a^2}{4} \left( \tilde{\rho}_n^2 + \frac{V_0^2}{a^4 \tilde{\rho}_n^2} \right) - \frac{V_0}{2}. \quad (21)$$

Using the identity

$$\frac{e^{2a(\beta-\beta_0)}}{[e^{2a(\beta-\beta_0)} + 1]^2} = \frac{1}{e^{2a(\beta-\beta_0)} + 1} - \frac{1}{[e^{2a(\beta-\beta_0)} + 1]^2}, \quad (22)$$

the potential of (12) can be rewritten as

$$V(\beta) = -\frac{V_0 + W}{e^{2a(\beta-\beta_0)} + 1} + \frac{W}{[e^{2a(\beta-\beta_0)} + 1]^2}. \quad (23)$$

### 2.3. Spectrum of the modified Woods-Saxon potential with centrifugal barrier

We remark that this potential has the same form as the potential of (11), with

$$V_0 + W = U_0 - \delta C_1, \quad W = \delta C_2, \quad (24)$$

leading to

$$V_0 = U_0 - \frac{4l(l+1)}{a\beta_0^3}, \quad W = \frac{12l(l+1)}{a^2\beta_0^4}. \quad (25)$$

Substituting these expressions in (21) and taking into account the first term in (11) the eigenvalues of the energy for the potential of (11) are found to be

$$E_n = \frac{l(l+1)}{\beta_0^2} \left( 1 + \frac{12a_0^2}{\beta_0^2} \right) - \left( \frac{\tilde{\rho}_n}{4a_0} \right)^2 - \left( \frac{U_0 a_0 - \frac{8l(l+1)a_0^2}{\beta_0^3}}{\tilde{\rho}_n} \right)^2 - \frac{U_0}{2}, \quad (26)$$

where

$$\tilde{\rho}_n = \sqrt{1 + \frac{192l(l+1)a_0^4}{\beta_0^4}} - (2n+1). \quad (27)$$

Therefore we have managed to obtain the energy eigenvalues of the WS potential with a repulsive barrier, as approximated through the Pekeris approximation, by exploiting the known solutions of the modified spherically symmetric WS potential, without having to solve the Schrödinger equation anew.

We remark that the condition of (20) leads to severe restrictions for  $n$ . Indeed, using (20) we have

$$b + c = \tilde{\rho}_n \geq 0, \quad (28)$$

which, using (27), leads to

$$n \leq \frac{1}{2} \left( -1 + \sqrt{1 + \frac{192l(l+1)a_0^4}{\beta_0^4}} \right). \quad (29)$$

Thus in the case of  $l = 0$ , only  $n = 0$  is allowed.

This result is valid in a 3-dimensional space. Following the same path one can see [67, 68] that the result is also valid in  $D$  dimensions, with the angular momentum  $l$  replaced by

$$l_D = l + \frac{D-3}{2}. \quad (30)$$

In the special case of a 5-dimensional space,  $l$  is replaced by

$$L = l + 1. \quad (31)$$

### 3. Bohr Hamiltonian for $\gamma$ -unstable nuclei

#### 3.1. Energy eigenvalues

The original Bohr Hamiltonian [6] is

$$H = -\frac{\hbar^2}{2B} \left[ \frac{1}{\beta^4} \frac{\partial}{\partial \beta} \beta^4 \frac{\partial}{\partial \beta} + \frac{1}{\beta^2 \sin 3\gamma} \frac{\partial}{\partial \gamma} \sin 3\gamma \frac{\partial}{\partial \gamma} - \frac{1}{4\beta^2} \sum_{k=1,2,3} \frac{Q_k^2}{\sin^2(\gamma - \frac{2}{3}\pi k)} \right] + V(\beta, \gamma), \quad (32)$$

where  $\beta$  and  $\gamma$  are the usual collective coordinates describing the shape of the nuclear surface,  $Q_k$  ( $k = 1, 2, 3$ ) are the components of angular momentum, and  $B$  is the mass parameter. In what follows we are going to consider  $\hbar^2 = 2B = 1$ .

Assuming that the potential depends only on the variable  $\beta$ , i.e.  $V(\beta, \gamma) = U(\beta)$ , one can proceed to separation of variables in the standard way [6, 7], using the wavefunction

$$\Psi(\beta, \gamma, \theta_i) = \frac{1}{\beta^2} f(\beta) \Phi(\gamma, \theta_i), \quad (33)$$

where  $\theta_i$  ( $i = 1, 2, 3$ ) are the Euler angles describing the orientation of the deformed nucleus in space.

In the equation involving the angles, the eigenvalues of the second order Casimir operator of SO(5) occur, having the form  $\Lambda = \tau(\tau + 3)$ , where  $\tau = 0, 1, 2, \dots$  is the quantum number characterizing the irreducible representations (irreps) of SO(5), called the “seniority” [69]. This equation has been solved by Bès [70].

The “radial” equation yields

$$-\frac{d^2 f}{d\beta^2} + \left( U(\beta) + \frac{(\tau + 1)(\tau + 2)}{\beta^2} \right) f(\beta) = E_{n,\tau} f(\beta). \quad (34)$$

The effective potential appearing in this equation coincides with that of (2), with the formal replacement of  $l$  by  $\tau + 1$ . Substituting in (26) we obtain the energy eigenvalues

$$E_{n,\tau} = \frac{(\tau + 1)(\tau + 2)}{\beta_0^2} \left( 1 + \frac{12a_0^2}{\beta_0^2} \right) - \left( \frac{\bar{\rho}_{n,\tau}}{4a_0} \right)^2 - \left( \frac{U_0 a_0 - \frac{8(\tau+1)(\tau+2)a_0^2}{\beta_0^3}}{\bar{\rho}_{n,\tau}} \right)^2 - \frac{U_0}{2}, \quad (35)$$

where

$$\bar{\rho}_{n,\tau} = \sqrt{1 + \frac{192(\tau + 1)(\tau + 2)a_0^4}{\beta_0^4}} - (2n + 1). \quad (36)$$

The restriction of (29) in this case reads

$$n \leq \frac{1}{2} \left( -1 + \sqrt{1 + \frac{192(\tau + 1)(\tau + 2)a_0^4}{\beta_0^4}} \right). \quad (37)$$

As we shall see in subsection 5.2, only  $n = 0$  is acceptable for the parameter values occurring in real nuclei. The violation of the condition of (37) even for  $n = 1$  has as a consequence to push the  $n = 1$  bands too low in energy, making them unphysical.



### 3.2. Rescaling the energy eigenvalues

Eq. (25) takes the form

$$U_0 = V_0 + \frac{8a_0(\tau + 1)(\tau + 2)}{\beta_0^3}, \quad (38)$$

implying that if  $V_0$  is a constant, then  $U_0$  depends on  $\tau$ , and vice versa. We are going to consider  $V_0$  as being the constant quantity. Then we can use this equation in order to eliminate  $U_0$  from (35). Using the notation

$$\tilde{A} = a_0/\beta_0, \quad (39)$$

the equation for the energy becomes

$$E_{n,\tau} = \frac{(\tau + 1)(\tau + 2)}{\beta_0^2} (1 + 12\tilde{A}^2 - 4\tilde{A}) - \frac{\bar{\rho}_{n,\tau}^2}{16a_0^2} - \frac{V_0^2 a_0^2}{\bar{\rho}_{n,\tau}^2} - \frac{V_0}{2}, \quad (40)$$

with

$$\bar{\rho}_{n,\tau} = \sqrt{1 + 192(\tau + 1)(\tau + 2)\tilde{A}^4 - (2n + 1)}. \quad (41)$$

In order to reduce the number of free parameters, we fit nuclear spectra leaving out overall scales, as it is done in the E(5) and X(5) models [1, 2]. Instead of fitting the raw experimental levels  $E_L$ , where  $L$  is the angular momentum, the quantities

$$\frac{E_L - E_0}{E_2 - E_0} \quad (42)$$

are used. In other words, the energy of the ground state is subtracted from all levels, and then each level is divided by the energy of the first excited state, which in even-even nuclei is the energy of the first excited state with  $L = 2$ . The connection between  $L$  and  $\tau$  is described in detail in subsection 3.4.

In the present case this has the following consequences on (40):

- 1) The last term,  $-V_0/2$ , plays no role, since it is a constant and cancels out.
- 2) Using the rescaling

$$\beta_0 = \frac{\tilde{\beta}_0}{\sqrt{V_0}}, \quad a_0 = \frac{\tilde{a}_0}{\sqrt{V_0}}, \quad (43)$$

a common factor  $V_0$  appears in all terms of (40), which therefore cancels out when (42) above is used.

3) Using  $\tilde{A} = a_0/\beta_0 = \tilde{a}_0/\tilde{\beta}_0$ , a common factor  $\tilde{\beta}_0^2$  can be taken away from the denominator of all terms of (40).

Then the equation to be used for the energy fits becomes

$$\bar{E}_{n,\tau} = (\tau + 1)(\tau + 2)(1 + 12\tilde{A}^2 - 4\tilde{A}) - \frac{\bar{\rho}_{n,\tau}^2}{16\tilde{A}^2} - \frac{\tilde{A}^2 \tilde{\beta}_0^4}{\bar{\rho}_{n,\tau}^2}, \quad (44)$$

where  $\bar{\rho}_{n,\tau}$  is still given by (41).

This is the equation used in the fits, from which the parameters  $\tilde{A}$  and  $\tilde{\beta}_0$  can be determined. Then  $\tilde{a}_0$  is calculated from  $\tilde{a}_0 = \tilde{A}\tilde{\beta}_0$ .

### 3.3. Fixing the scale

The Woods–Saxon potential is essentially different from zero within its radius, which in this case is  $\beta_0$ .

One way to fix the scale is to identify the radius of the potential,  $\beta_0$ , with the  $\beta_{exp}$  value obtained from the experimental values of  $B(E2; 0_1^+ \rightarrow 2_1^+)$  [71]. Then from (43) one simply has

$$V_0 = \frac{\tilde{\beta}_0^2}{\beta_{exp}^2}. \quad (45)$$

Notice that in this case  $a_0$  can be calculated directly from  $a_0 = \tilde{A}\beta_{exp}$ .

It should be recalled at this point that while the  $B(E2; 0_1^+ \rightarrow 2_1^+)$  values are experimental quantities which are model independent, the deformation parameter is model dependent [71]. In the present case, a uniform charge distribution out to the distance  $R(\theta, \phi)$  is assumed, with zero charge beyond it, while the nuclear radius is taken to be  $R_0 = 1.2 A^{1/3}$  fm. Then the deformation is connected to the transition probability by

$$\beta = \frac{4\pi}{3ZR_0^2} \sqrt{\frac{B(E2; 0_1^+ \rightarrow 2_1^+)}{e^2}}, \quad (46)$$

where  $B(E2; 0_1^+ \rightarrow 2_1^+)$  is measured in  $e^2b^2$ . It should be noticed that  $\beta$  is the deformation parameter defined in the Bohr framework [6]. A slightly different deformation parameter  $\varepsilon$  is used in the framework of the Nilsson model [72], connected to the Bohr parameter by  $\varepsilon = 0.946\beta$  (see p. 125 of [72], or eq. (2.82) of [73]).

### 3.4. The spectrum

The spectrum is characterized by the  $O(5) \supset SO(3)$  symmetry [69, 70].  $\tau$  and  $L$  are the quantum numbers characterizing the irreps of  $O(5)$  and  $SO(3)$  respectively. The values of angular momentum  $L$  contained in each irrep of  $O(5)$  (i.e. for each value of  $\tau$ ) are given by the algorithm [74]

$$\tau = 3\nu_\Delta + \lambda, \quad \nu_\Delta = 0, 1, \dots, \quad (47)$$

$$L = \lambda, \lambda + 1, \dots, 2\lambda - 2, 2\lambda \quad (48)$$

(with  $2\lambda - 1$  missing), where  $\nu_\Delta$  is the missing quantum number in the reduction  $O(5) \supset SO(3)$ , and are listed in Table 1.

The ground state band (gsb) has  $n = 0$  and levels  $L_g = 0, 2, 4, 6, \dots$ , for which  $\nu_\Delta = 0$  and  $L_g = 2\tau$ . Thus within the gsb one has

$$(\tau + 1)(\tau + 2) = \frac{(L + 2)(L + 4)}{4}. \quad (49)$$

The quasi- $\gamma_1$  band has  $n = 0$  and levels with  $L_\gamma = 2, 3, 4, 5, \dots$ , which are characterized by  $\nu_\Delta = 0$  and  $L_\gamma = 2\tau - 2$  for  $L_\gamma$  being even, or by  $L_\gamma = 2\tau - 3$  for  $L_\gamma$  being odd. Therefore they exhibit the following degeneracies

$$2_\gamma = 4_g, \quad 3_\gamma = 4_\gamma = 6_g, \quad 5_\gamma = 6_\gamma = 8_g, \quad 7_\gamma = 8_\gamma = 10_g, \dots \quad (50)$$

The quasi- $\beta_1$  band has levels  $L_\beta = 0, 2, 4, 6, \dots$ . There are two choices:

1)  $n = 0$ , in which the levels have  $\nu_\Delta = 1$  and  $L_\beta = 2\tau - 6$ , leading to the following degeneracies

$$0_\beta = 6_g, \quad 2_\beta = 8_g, \quad 4_\beta = 10_g, \quad 6_\beta = 12_g, \dots \quad (51)$$

2)  $n = 1$ , in which the levels have  $\nu_\Delta = 0$  and  $L_\beta = 2\tau$ . Then no degeneracies of this kind occur.

## 4. Bohr Hamiltonian for prolate deformed nuclei

### 4.1. Energy eigenvalues

If the potential has a minimum around  $\gamma = 0$ , as it is the case for prolate deformed nuclei, the angular momentum term in (32) can be written [2] as

$$\sum_{k=1}^3 \frac{Q_k^2}{\sin^2(\gamma - \frac{2\pi}{3}k)} \approx \frac{4}{3}(Q_1^2 + Q_2^2 + Q_3^2) + Q_3^2 \left( \frac{1}{\sin^2 \gamma} - \frac{4}{3} \right). \quad (52)$$

Exact separation of  $\beta$  from the rest of the variables can be obtained for potentials of the form [7, 5]

$$U(\beta, \gamma) = u(\beta) + \frac{v(\gamma)}{\beta^2}. \quad (53)$$

Concerning the  $\gamma$  and Euler angles, the solution provided by Bès [70] is not valid any more, thus we seek, as is customary in the literature (see Chapter IV of the review article [5] for further details) wave functions of the form

$$\psi(\beta, \gamma, \theta_j) = \xi_L(\beta) \Gamma_K(\gamma) \mathcal{D}_{M,K}^L(\theta_j), \quad (54)$$

where  $\theta_j$  ( $j = 1, 2, 3$ ) are the Euler angles,  $\mathcal{D}(\theta_j)$  represents Wigner functions of these angles,  $L$  stands for the eigenvalues of the angular momentum, while  $M$  and  $K$  are the eigenvalues of the projections of the angular momentum on the laboratory-fixed  $z$ -axis and the body-fixed  $z'$ -axis respectively. In these wave functions the dependence on the Euler angles is entering through the Wigner functions, as in the many examples reviewed in [5], while  $K$  is assumed to be a good quantum number, an assumption which is not *a priori* justified, since strong  $K$  mixing can be present.

The  $\gamma$ -equation occurring from this separation of variables has been solved in [12], using a potential

$$v(\gamma) = (3c)^2 \gamma^2, \quad (55)$$

its eigenfunctions written in terms of Laguerre polynomials and its energy eigenvalues given by

$$\epsilon_\gamma = (3C)(n_\gamma + 1), \quad C = 2c, \quad n_\gamma = 0, 1, 2, 3, \dots, \quad (56)$$

while the separation constant is

$$\lambda = \epsilon_\gamma - \frac{K^2}{3}. \quad (57)$$

It should be noticed at this point that the  $\gamma$  potential used in the Bohr Hamiltonian has to be periodic in  $\gamma$  [6, 33, 75]. The potential of (55), used in several solutions [2, 5, 12] is a lowest order approximation, representing the first  $\gamma$ -dependent term in the Taylor expansion of the proper periodic potential. There has been recently extensive work involving proper periodic  $\gamma$  potentials in the Bohr Hamiltonian [5, 48, 76, 77, 78, 79, 80, 81].

The radial equation takes the form [12]

$$\left[ -\frac{1}{\beta^4} \frac{\partial}{\partial \beta} \beta^4 \frac{\partial}{\partial \beta} + \frac{L(L+1)}{3\beta^2} + \frac{\lambda}{\beta^2} + u(\beta) \right] \xi_L(\beta) = \epsilon \xi_L(\beta). \quad (58)$$

Transforming  $\xi_L$  into  $\chi_L$  by the relation

$$\xi_L(\beta) = \frac{\chi_L(\beta)}{\beta^2}, \quad (59)$$

we obtain

$$\chi_L''(\beta) + \left[ \epsilon - \frac{\frac{L(L+1)}{3} + \lambda + 2}{\beta^2} - u(\beta) \right] \chi_L(\beta) = 0. \quad (60)$$

We remark that this equation looks very similar to (34), with  $\frac{L(L+1)}{3} + \lambda + 2$  replacing  $(\tau + 1)(\tau + 2)$ . Therefore from (35) we see that the energy eigenvalues become

$$E_{n,L} = \frac{\left( \frac{L(L+1)}{3} + \lambda + 2 \right)}{\beta_0^2} \left( 1 + \frac{12a_0^2}{\beta_0^2} \right) - \left( \frac{\tilde{\rho}_{n,L}}{4a_0} \right)^2 - \left( \frac{U_0 a_0 - \frac{8 \left( \frac{L(L+1)}{3} + \lambda + 2 \right) a_0^2}{\beta_0^3}}{\tilde{\rho}_{n,L}} \right)^2 - \frac{U_0}{2}, \quad (61)$$

where

$$\tilde{\rho}_{n,L} = \sqrt{1 + 192 \left( \frac{L(L+1)}{3} + \lambda + 2 \right) \frac{a_0^4}{\beta_0^4}} - (2n + 1). \quad (62)$$

The restriction of (29) in this case reads

$$n \leq \frac{1}{2} \left( -1 + \sqrt{1 + 192 \left( \frac{L(L+1)}{3} + \lambda + 2 \right) \frac{a_0^4}{\beta_0^4}} \right). \quad (63)$$

As we shall see in subsection 5.1, only  $n = 0$  is acceptable for the parameter values occurring in real nuclei. The violation of the condition of (63) even for  $n = 1$  has as a consequence the failure of the relevant fitting attempts.

#### 4.2. Rescaling the energy eigenvalues

Following the same rescaling procedure as in the  $\gamma$ -unstable case, the equation used in the fits becomes

$$\bar{E}_{n,L} = \left( \frac{L(L+1)}{3} + \lambda + 2 \right) (1 + 12\tilde{A}^2 - 4\tilde{A}) - \frac{\tilde{\rho}_{n,L}^2}{16\tilde{A}^2} - \frac{\tilde{A}^2 \tilde{\beta}_0^4}{\tilde{\rho}_{n,L}^2}, \quad (64)$$

where

$$\tilde{\rho}_{n,L} = \sqrt{1 + 192 \left( \frac{L(L+1)}{3} + \lambda + 2 \right) \tilde{A}^4} - (2n + 1). \quad (65)$$

This is the equation used in the fits, from which the parameters  $\tilde{A}$ ,  $\tilde{\beta}_0$ , and  $C$  (appearing in  $\lambda$ ) can be determined.

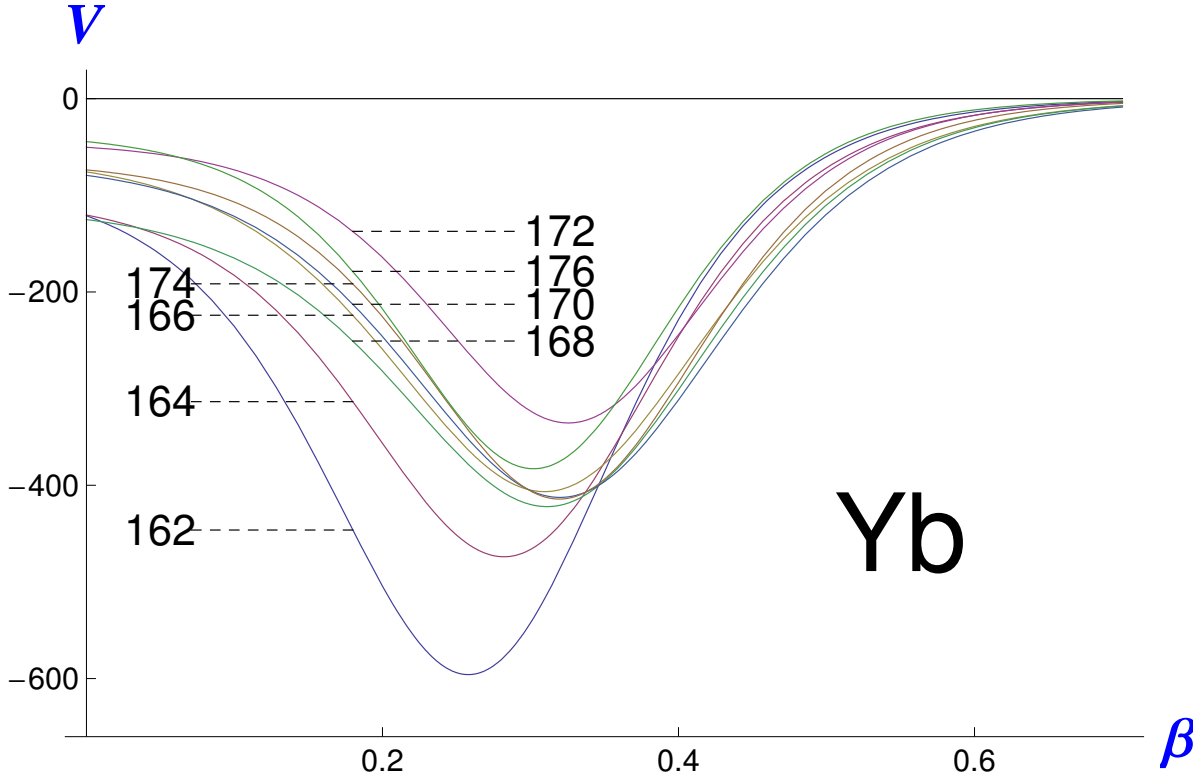


**Figure 3.** (Color online) Effective potentials for  $L = 10$  for some Yb isotopes, obtained from (23). The parameters are taken from Table 2, while  $W$  is given by (25) with  $l(l+1)$  replaced by  $\frac{L(L+1)}{3} + \lambda + 2$ , where  $\lambda = 3C$  from (57) and (56). The quantities shown are dimensionless.

## 5. Numerical results

### 5.1. Prolate deformed nuclei

As a first test, the spectra of 63 nuclei with  $R_{4/2} > 2.9$  have been fitted. The quality measure

$$\sigma_N = \sqrt{\frac{\sum_{i=1}^N (E_i(\text{exp}) - E_i(\text{th}))^2}{(N-1)(E(2_1^+))^2}}, \quad (66)$$

has been used in the rms fits.

The results for 46 nuclei are shown in Table 2. The following comments apply.

1) Only the ground state band and the quasi- $\gamma_1$  band have been included in the fits.

2) When trying to include the quasi- $\beta_1$  band in the fits, trying to correspond it to the  $n = 1$  case, the fits fail. The failure is due to violation of the condition of (63).

The parameters obtained from fitting the experimental spectra of  $^{162-176}\text{Yb}$ , shown in Table 2, exhibit the following features.

1) The depth of the potential,  $V_0$ , exhibits a clear minimum near the middle of the neutron shell ( $^{174}\text{Yb}_{104}$ ), where maximum deformation is observed, as indicated by the clear maximum exhibited by  $\beta_0 \equiv \beta_{exp}$ , the experimental values of deformation obtained from the  $B(E2; 0^+ \rightarrow 2^+)$  [71].

2) The highest diffuseness  $\tilde{a}_0$  occurs nearest to the shell closure, while the lowest appears near the middle of the shell.

3) In retrospect, the selection of the parameters used in the fits was physically meaningful.  $\tilde{\beta}_0$  is related to the “well size” [24], while  $\tilde{A}$  is related to the ratio of the diffuseness parameter  $a_0$  over the average width of the potential  $\beta_0$ .

4) The potentials obtained from the Yb isotopes are shown in figure 3, corroborating the above made remarks about maximum depth and diffuseness nearest to the shell closure, and minimum depth and diffuseness near the middle of the shell. We remark that the dip near the surface of the modified spherically symmetric WS potential is becoming very large, dominating the overall shape of the potential. It is instructive to compare the shapes of the potentials appearing in figure 3 to these in figure 2, since they come from (23) and (12) respectively, which are equivalent.

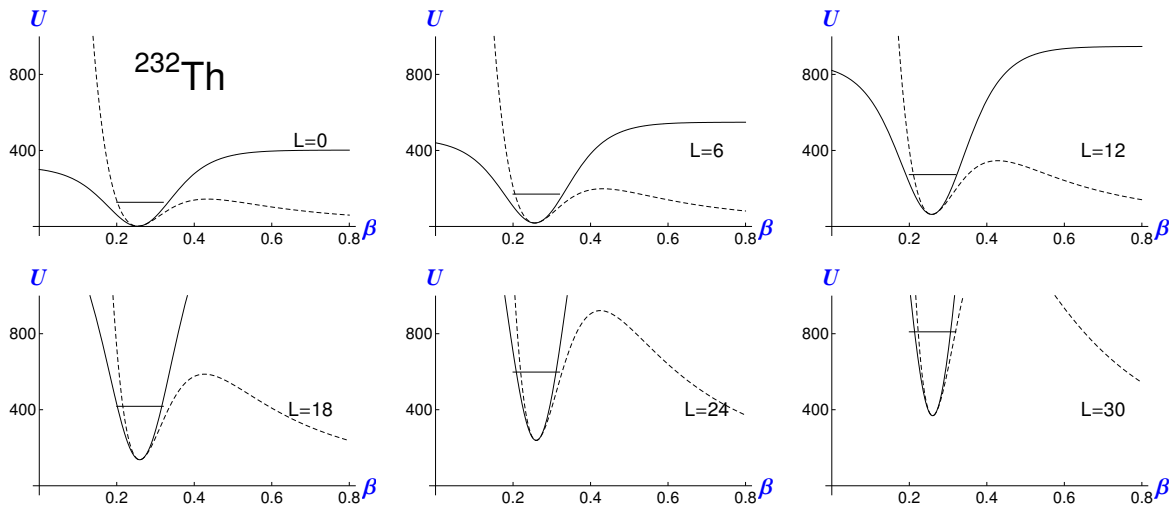


**Figure 4.** (Color online) Exact (dashed lines) and approximate (solid lines) effective potentials for  $L = 0, 6, 12, 18, 24, 30$  for  $^{232}\text{Th}$ , obtained from (2) and (11) respectively. The parameters are taken from Table 2, providing the quantities needed from (5), (9), and (10) while  $U_0$  is given by (25) with  $l(l+1)$  replaced by  $\frac{L(L+1)}{3} + \lambda + 2$ , where  $\lambda = 3C$  from (57) and (56). The corresponding energy levels, determined from (61), are also shown. The quantities shown are dimensionless. See subsection 5.1 for further discussion.

The spectra obtained for some rare earths and actinides are shown in Table 3. Good agreement with the data is obtained.

A question arising at this point is the accuracy of the Pekeris approximation used in the derivation of the relevant formulae. In order to check this, we show in figure 4

both the original exact potential (dashed lines), obtained from (2), and the approximate potential (solid lines) occurring after the Pekeris approximation, obtained from (11), for six different values of the angular momentum  $L$ , in the case of  $^{232}\text{Th}$ . In addition, the relevant energy levels, obtained from (61), are shown. The following comments apply.

1) Near their bottoms, the exact and the approximate potentials nearly coincide. They exhibit minima very close to each other, while in addition the two potentials form similar wells around the minima.

2) At higher energies, the approximate potential wells are slightly displaced to the left, in relation to the exact potentials. However, at the energy of main interest, i.e. at the energy of the relevant level, the widths of the two potentials are nearly equal.

3) The approximation appears to be better at higher values of  $L$ , i.e. at higher energy levels. This is expected, since the fits were obtained through an rms procedure.

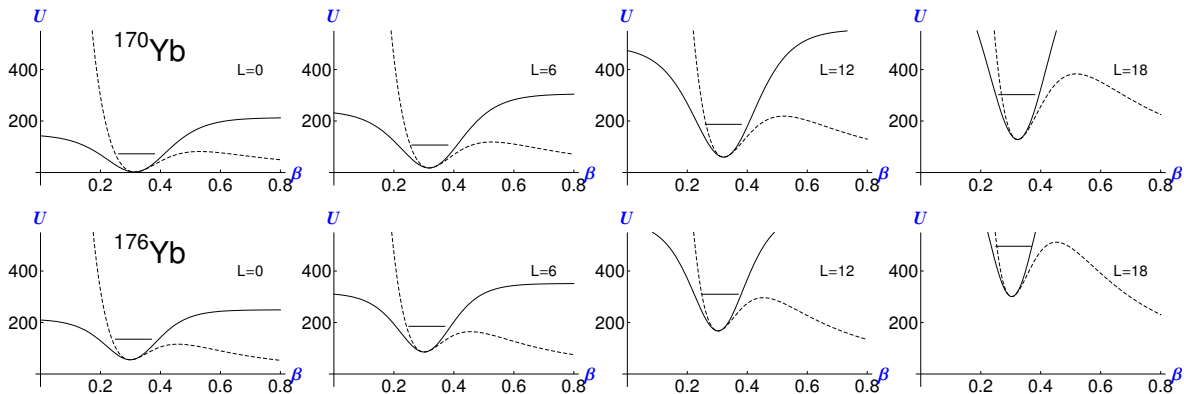


**Figure 5.** (Color online) Same as figure 4, but for  $L = 0, 6, 12, 18$ , for  $^{170}\text{Yb}$  (a) and  $^{176}\text{Yb}$  (b). See subsection 5.1 for further discussion.

The same observations hold for all nuclei shown in Table 2, with two exceptions,  $^{172}\text{Yb}$  and  $^{176}\text{Yb}$ , the latter exhibited in figure 5. While  $^{170}\text{Yb}$  (and the rest of the Yb isotopes shown in Table 2) exhibit the qualitative behaviour described above, in  $^{176}\text{Yb}$  (as well as in  $^{172}\text{Yb}$ ) we remark that the approximation breaks down, since for the lowest values of  $L$  the relevant energy level lies higher than the corresponding barrier on the rhs of the exact potential. In other words, we still get fits of good quality, which are obtained using the approximate potential, but this potential is not similar to the exact potential any more, preventing us to draw any conclusions regarding the exact potential. It should be noticed at this point that the approximate potentials (solid lines) for Yb isotopes shown in figures 3 and 5 are identical, up to a displacement by a constant. Indeed, the potentials of figure 3 come from (23), while the potentials of figure 5 come from (11), the latter being displaced in relation to the former by the term  $\delta C_0$ . This term is included in figure 5, since it is necessary for the comparison to the exact potentials (dashed lines) given by (2).

$^{172}\text{Yb}$  and  $^{176}\text{Yb}$  are not isolated cases. Similar breakdowns of the approximation have been found in 17 more nuclei, shown in Table 4. In all cases, good fits of quality

comparable to those shown in Table 2 are obtained, but they correspond to approximate potentials being very different from the exact ones.

From the numerical results obtained for all the nuclei mentioned above, we see that the breakdown of the approximation occurs for “well size”  $\tilde{\beta}_0 \leq 1.8$  and/or diffuseness  $\tilde{a}_0 \leq 0.43$ . Since  $\beta_0^2$  appears in the denominator of the rotational term, this result is understandable. The lower  $\beta_0$  becomes, the more important the rotational term, in which the Pekeris approximation has been used, becomes, thus the approximation to the exact potential deteriorates.

We therefore conclude that good fits are obtained for all nuclei studied, but only if the “well size”  $\tilde{\beta}_0$  fulfils the condition  $\tilde{\beta}_0 \geq 1.9$  and the diffuseness fulfils the condition  $\tilde{a}_0 \geq 0.44$  the approximate potentials are quite similar to the corresponding exact potentials.

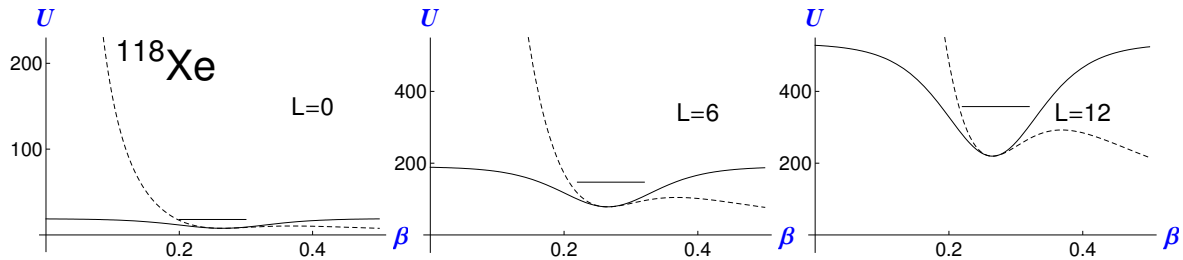


**Figure 6.** (Color online) Exact (dashed lines) and approximate (solid lines) effective potentials for  $\tau = 0, 3, 6$  ( $L = 0, 6, 12$ ) for  $^{118}\text{Xe}$ , obtained from (2) and (11) respectively. The parameters are taken from Table 5, providing the quantities needed from (5), (9), and (10), while  $W$  is given by (25) with  $l(l+1)$  replaced by  $(\tau+1)(\tau+2)$ . The corresponding energy levels, determined from (40), are also shown. The quantities shown are dimensionless. See subsection 5.2 for further discussion.

## 5.2. $\gamma$ -unstable nuclei

The spectra of 38 nuclei with  $R_{4/2} < 2.6$  [ $^{98,100,102}\text{Ru}$ ,  $^{102,104,106,108,110,112,114,116}\text{Pd}$ ,  $^{108,110,112}\text{Cd}$ ,  $^{118,120,122,124,126,128,130,132,134}\text{Xe}$ ,  $^{130,132,134}\text{Ba}$ ,  $^{134,138}\text{Ce}$ ,  $^{142}\text{Gd}$ ,  $^{156}\text{Er}$ ,  $^{186,188,190,192,194,196,198,200}\text{Pt}$ ] have been fitted, using the same quality measure.

The following comments apply.

1) Only the ground state band and the quasi- $\gamma_1$  band have been included in the fits.

2) When trying to include the quasi- $\beta_1$  band in the fits, trying to correspond it to the  $n = 1$  case, one finds it lying too low in energy, due to the violation of the restriction of (37).

3) When trying to include the quasi- $\beta_1$  band in the fits, trying to correspond it to the  $n = 0$  case, the levels of the  $\beta_1$ -band in most cases are overestimated. There is nothing to be done against this, since the degeneracies of (51) fix the position of the theoretical levels. Thus this failure is due to the fact that the experimental data do not exhibit exactly the  $O(5)$  degeneracies.



The parameters obtained from fitting the experimental spectra of  $^{118-134}\text{Xe}$ , shown in Table 5. We remark that in all cases the “well size”  $\tilde{\beta}_0$  is much lower than 1.8, while in addition the diffuseness is much lower than 0.43. The same holds for all of the 38 nuclei considered. Therefore the approximate potentials bear little relevance to the exact potentials.

As an example, we show in figure 6 both the original exact potential (broken lines), obtained from (2), and the approximate potential (solid lines) occurring after the Pekeris approximation, obtained from (11), for three different values of the seniority quantum number  $\tau$ , in the case of  $^{118}\text{Xe}$ . In addition, the relevant energy levels, obtained from eq. (40), are shown. The following comments apply.

- 1) Near their bottoms, the exact and the approximate potentials nearly coincide.
- 2) The approximation breaks down, since for all values of  $\tau$  the relevant energy level lies higher than the relevant barrier on the rhs of the exact potential. We still get fits of good quality, which are obtained using the approximate potential, but this potential is not similar to the exact potential any more, preventing us to draw any conclusions regarding the exact potential.

We therefore conclude that although we could derive analytical expressions for fitting the spectra, the parameter values coming out from the fits correspond to “well sizes” and diffuseness for which the approximate potential is not quite similar to the exact potential, i.e. the Pekeris approximation breaks down.

## 6. Conclusions

The main results are summarized here.

- 1) Approximate solutions in closed form are obtained for the 5-dimensional Bohr Hamiltonian with the Woods–Saxon potential, using the Pekeris approximation and the exact solutions of an extended Woods–Saxon potential in one dimension, featuring a dip near its surface.

- 2) Applying the results to several  $\gamma$ -unstable and prolate deformed nuclei, we find that the WS potential can describe the ground state bands and the  $\gamma_1$  bands equally well as other potentials (Davidson, Kratzer, Morse), if the “well size” and the diffuseness are large enough (at least 1.9 and 0.44 respectively), but it fails to describe the  $\beta_1$  bands, apparently because of its lack of a hard core. Several (forty-four) examples of deformed nuclei satisfying this condition have been found, but on the other hand all  $\gamma$ -unstable nuclei considered violate this condition.

- 3) The form of the potentials coming out from the fits exhibits a very large dip near the surface. In other words, the Bohr equation forces the parameters of the WS potential to obtain values producing a very large dip near its surface, so that its overall shape around its minimum largely resembles the shape around the minimum of the Davidson, or the Kratzer, or the Morse potential.

- 4) The present results suggest that potentials used in the Bohr Hamiltonian can provide satisfactory results for nuclear spectra if they possess two features, a hard core

and a deep oscillator-like minimum. They also suggest that the lack of a hard core does not decisively affect the description of the ground state and  $\gamma_1$  bands, but destroys the ability of the potential to describe  $\beta_1$  bands.

Concerning the position of the quasi- $\beta_1$  bands, which are not reproduced by the Woods–Saxon potential, the following comments apply.

1) The quasi- $\beta_1$  bandheads move to higher energies (normalized to the energy of the first excited state) both in  $\gamma$ -unstable and in deformed nuclei, if the left wall of the infinite well potential used in the E(5) and X(5) critical point symmetries is gradually moved to the right of the origin of the  $\beta$ -axis, approaching the right wall [82, 83].

2) The interlevel spacings within the  $\beta_1$ - band, which are known to be overestimated in the framework of the X(5) critical point symmetry, get fixed by allowing the right wall of the infinite well potential to be sloped to the right [84]. It should be mentioned here that the identification of a symmetry underlying the X(5) special solution of the Bohr Hamiltonian remains an open problem.

Analytical wave functions for the Bohr Hamiltonian with the WS potential can be readily obtained by exploiting the similarity of this Hamiltonian, after using the Pekeris approximation, to the exactly soluble extended WS potential with a dip near its surface. The calculation of B(E2) transition rates becomes then a straightforward task, to be addressed in further work.

Finally, the solution of the Bohr Hamiltonian with a Woods–Saxon potential within the framework of the algebraic collective model [41, 42, 43, 44] would offer the opportunity of comparison of the present approximate results to exact numerical solutions.

## Acknowledgments

B. Gönül and M. Çapak acknowledge financial support by the Scientific and Technical Research Council of Turkey (TÜBİTAK) under project number ARDEB/1002-113F218.

D. Petrellis acknowledges financial support by the Scientific Research Projects Coordination Unit of Istanbul University under Project No 50822.

## References

- [1] Iachello F 2000 *Phys. Rev. Lett.* **85** 3580
- [2] Iachello F 2001 *Phys. Rev. Lett.* **87** 052502
- [3] Cejnar P, Jolie J and Casten R F 2010 *Rev. Mod. Phys.* **82** 2155
- [4] Casten R F and E. A. McCutchan E A 2007 *J. Phys. G: Nucl. Part. Phys.* **34** R285
- [5] Fortunato L 2005 *Eur. Phys. J. A* **26** 1
- [6] Bohr A 1952 *Mat. Fys. Medd. K. Dan. Vidensk. Selsk.* **26** no. 14
- [7] Wilets L and Jean M 1956 *Phys. Rev.* **102** 788
- [8] Bohr A and Mottelson B R 1975 *Nuclear Structure Vol. II: Nuclear Deformations* (Benjamin, New York)
- [9] Davidson P M 1932 *Proc. R. Soc. London Ser. A* **135** 459
- [10] Rohoziński S G, Srebrny J and Horbaczewska K 1974 *Z. Phys.* **268** 401

- [11] Elliott J P, Evans J A and Park P 1986 *Phys. Lett. B* **169** 309
- [12] Bonatsos D, McCutchan E A, Minkov N, Casten R F, Yotov P, Lenis D, Petrellis D and Yigitoglu I 2007 *Phys. Rev. C* **76** 064312
- [13] Bonatsos D, Georgoudis P E, Lenis D, Minkov N and Quesne C 2011 *Phys. Rev. C* **83** 044321
- [14] Kratzer A 1920 *Z. Phys.* **3** 289
- [15] Fortunato L and Vitturi A 2003 *J. Phys. G: Nucl. Part. Phys.* **29** 1341
- [16] Fortunato L and Vitturi A 2004 *J. Phys. G: Nucl. Part. Phys.* **30** 627
- [17] Bonatsos D, Georgoudis P E, Minkov N, Petrellis D and Quesne C 2013 *Phys. Rev. C* **88** 034316
- [18] Morse P M 1929 *Phys. Rev.* **34** 57
- [19] Boztosun I, D. Bonatsos D and Inci I 2008 *Phys. Rev. C* **77** 044302
- [20] Inci I, Bonatsos D, Boztosun I 2011 *Phys. Rev. C* **84** 024309
- [21] Brookhaven National Laboratory, National Nuclear Data Center, <http://www.nndc.bnl.gov/ensdf/>
- [22] Woods R D and Saxon D S 1954 *Phys. Rev.* **95** 577
- [23] Heyde K 1994 *Basic Ideas and Concepts in Nuclear Physics* (IOP, Bristol)
- [24] Caprio M A 2002 *Phys. Rev. C* **65** 031304(R)
- [25] Inci I, Boztosun I and Gonen Y E 2012 *J. Phys. G: Nucl. Part. Phys.* **39** 085112
- [26] Gönül B and Köksal K 2007 *Phys. Scr.* **76** 565
- [27] Flügge S 1974 *Practical Quantum Mechanics* (Springer-Verlag, Heidelberg)
- [28] Pekeris C L 1934 *Phys. Rev.* **45** 98
- [29] Koura H and Yamada M 2000 *Nucl. Phys. A* **671** 96
- [30] Faessler A and Greiner W 1962 *Z. Phys.* **168** 425
- [31] Faessler A, Greiner W, and Sheline R K 1965 *Nucl. Phys.* **70** 33
- [32] Kumar K 1963 Ph.D. thesis, Carnegie Institute of Technology
- [33] Kumar K and Baranger M 1967 *Nucl. Phys. A* **92** 608
- [34] Gneuss G and Greiner W 1971 *Nucl. Phys. A* **171** 449
- [35] Hecht K T 1965 *Nucl. Phys.* **63** 177
- [36] Hess P O, Seiwert M, Maruhn J, and Greiner W 1980 *Z. Phys. A* **296** 147
- [37] Hess P O, Maruhn J, and Greiner W 1981 *J. Phys. G: Nucl. Phys.* **7** 737
- [38] Chacón E, Moshinsky M, and Sharp R T 1976 *J. Math. Phys.* **17** 668
- [39] Chacón E and Moshinsky M 1977 *J. Math. Phys.* **18** 870
- [40] Rowe D J and Bahri C 1998 *J. Phys. A: Math. Gen.* **31** 4947
- [41] Rowe D J 2004 *Nucl. Phys. A* **735** 372
- [42] Rowe D J and Turner P S 2005 *Nucl. Phys. A* **753** 94
- [43] Caprio M A 2009 *Phys. Lett. B* **672** 396
- [44] Rowe D J, Welsh T A, and Caprio M A 2009 *Phys. Rev. C* **79** 054304
- [45] Davydov A S and Filippov G F 1958 *Nucl. Phys.* **8** 237
- [46] Davydov A S and Rostovsky V S 1959 *Nucl. Phys.* **12** 58
- [47] Yigitoglu I and Bonatsos D 2011 *Phys. Rev. C* **83** 014303
- [48] Raduta A A and Baganu P 2011 *Phys. Rev. C* **83** 034313
- [49] Inci I 2014 *Int. J. Mod. Phys. E* **23** 1450053
- [50] Baganu P and Budaca R 2015 *Phys. Rev. C* **91** 014306
- [51] Kumar K and Baranger M 1968 *Nucl. Phys. A* **122** 273
- [52] Kaniowska T, Sobiczewski A, Pomorski K, and Rohozlaski S G 1976 *Nucl. Phys. A* **274** 151
- [53] Rohoziński S G, Dobaczewski J, Nerlo-Pomorska B, Pomorski K, and Srebrny J 1977 *Nucl. Phys. A* **292** 66
- [54] Próchniak L and Rohoziński S G 2009 *J. Phys. G: Nucl. Part. Phys.* **36** 123101
- [55] Nikšić T, Li Z P, Vretenar D, Próchniak L, Meng J, and Ring P 2009 *Phys. Rev. C* **79** 034303
- [56] Li Z P, Nikšić T, Vretenar D, Meng J, Lalazissis G A, and Ring P 2009 *Phys. Rev. C* **79** 054301
- [57] Li Z P, Nikšić T, Vretenar D, and Meng J 2010 *Phys. Rev. C* **81** 034316
- [58] Li Z P, Nikšić T, Vretenar D, Ring P, and Meng J 2010 *Phys. Rev. C* **81** 064321
- [59] Berkdemir C and Han J 2005 *Chem. Phys. Lett.* **409** 203

- [60] Bayrak O and Boztosun I 2007 *J. Phys. A: Math. Theor.* **40** 11119
- [61] Morales D A 2004 *Chem. Phys. Lett.* **394** 68
- [62] Dong S, García-Ravelo J and Dong S -H 2007 *Phys. Scr.* **76** 393
- [63] Bera P K 2012 *Pramana J. Phys.* **78** 91
- [64] Ferreira F J S and Prudente F V 2013 *Phys. Lett. A* **377** 3027
- [65] Wei G -F and Dong S -H 2010 *Eur. Phys. J. A* **46** 207
- [66] Abramowitz M and Stegun I A 1965 *Handbook of Mathematical Functions* (Dover, New York)
- [67] Badalov V H, Ahmadov H I, and Badalov S V 2009 *Int. J. Mod. Phys. E* **18** 631
- [68] Badalov V H and Ahmadov H I 2011 arXiv:1111.4734 [math-ph]
- [69] Rakavy G 1957 *Nucl. Phys.* **4** 289
- [70] Bès D R 1959 *Nucl. Phys.* **10** 373
- [71] Raman S, Nestor Jr. C W, and Tikkanen P 2001 *At. Data Nucl. Data Tables* **78** 1
- [72] Nilsson S G and Ragnarsson I 1995 *Shapes and Shells in Nuclear Structure* (Cambridge University Press, Cambridge)
- [73] Ring P and Schuck P 1980 *The Nuclear Many-Body Problem* (Springer, Berlin)
- [74] Iachello F and Arima A 1987 *The Interacting Boson Model* (Cambridge University Press, Cambridge)
- [75] Corrigan T M, Margetan F J, and Williams S A 1976 *Phys. Rev. C* **14** 2279
- [76] De Baerdemacker S, Fortunato L, Hellemans V, and Heyde K 2006 *Nucl. Phys. A* **769** 16
- [77] Gheorghe A C, Raduta A A, and Faessler A 2007 *Phys. Lett. B* **648** 171
- [78] Raduta A A, Gheorghe A C, Buganu P, and Faessler A 2009 *Nucl. Phys. A* **819** 46
- [79] Raduta A A, Buganu P, and Faessler A 2012 *J. Phys. G: Nucl. Part. Phys.* **39** 025103
- [80] Raduta A A and Buganu P 2013 *J. Phys. G: Nucl. Part. Phys.* **40** 025108
- [81] Raduta A A and Buganu P 2013 *Phys. Rev. C* **88** 064328
- [82] Pietralla N and Gorbachenko O M 2004 *Phys. Rev. C* **70** 011304(R)
- [83] Bonatsos D, Lenis D, Pietralla N, and Terziev P A 2006 *Phys. Rev. C* **74** 044306
- [84] Caprio M A 2004 *Phys. Rev. C* **69** 044307

**Table 1.** Quantum numbers appearing in the  $O(5) \supset SO(3)$  reduction [74], occurring from (47) and (48).

$\tau$	$\nu_\Delta$	$\lambda$	$L$
0	0	0	0
1	0	1	2
2	0	2	4,2
3	0	3	6,4,3
3	1	0	0
4	0	4	8,6,5,4
4	1	1	2
5	0	5	10,8,7,6,5
5	1	2	4,2
6	0	6	12,10,9,8,7,6
6	1	3	6,4,3
6	2	0	0

**Table 2.** Comparison of theoretical predictions of the Bohr Hamiltonian with the Woods–Saxon potential for 46 axially symmetric prolate deformed nuclei to experimental data [21] of rare earth and actinides with  $R_{4/2} > 2.9$  and known  $0_2^+$  and  $2_\gamma^+$  states. The angular momenta of the highest levels of the ground state and  $\gamma_1$  bands included in the rms fit are labelled by  $L_g$  and  $L_\gamma$  respectively, while  $N$  indicates the total number of levels involved in the fit and  $\sigma$  is the quality measure of (66). All energies are normalized to the energy of the first excited state,  $E(2_1^+)$ . For each band, the  $R_{4/2} = E(4_1^+)/E(2_1^+)$  ratio (labelled by 4/2), the normalized bandhead of the  $\gamma_1$  band (labelled as  $2_\gamma/2$ ), and the normalized last members of the ground state and  $\gamma_1$  bands included in the fit (labelled by  $L_g/2$  and  $L_\gamma/2$  respectively), are reported.  $\beta_0$  has been obtained from [71]. The theoretical predictions are obtained from (64). See subsection 5.1 for further discussion.

nucleus	$\tilde{\beta}_0$	$\tilde{A}$	$C$	$\tilde{a}_0$	$\beta_0$	$V_0$	$10^3 a_0$	$L_g$	$L_\gamma$	$N$	$\sigma$	4/2 exp	4/2 th	$L_g/2$ exp	$L_g/2$ th	$2_\gamma/2$ exp	$2_\gamma/2$ th	$L_\gamma/2$ exp	$L_\gamma/2$ th
<sup>150</sup> Nd	4.1	0.15	7.6	0.62	0.285	207	43	14	4	9	0.24	2.93	3.02	20.6	20.7	8.2	8.6	10.4	9.9
<sup>152</sup> Sm	4.8	0.20	8.6	0.96	0.306	245	61	16	9	15	0.60	3.01	3.10	27.6	28.0	8.9	10.2	19.5	18.4
<sup>154</sup> Sm	4.2	0.22	14.0	0.92	0.341	152	75	16	7	13	0.53	3.25	3.26	36.2	36.5	17.6	18.6	26.3	25.0
<sup>154</sup> Gd	3.4	0.24	6.9	0.82	0.312	119	75	26	7	18	0.35	3.02	3.14	57.3	57.4	8.1	8.8	14.7	14.2
<sup>156</sup> Gd	2.2	0.24	10.8	0.53	0.338	42	81	26	16	27	0.68	3.24	3.25	74.0	74.1	13.0	14.5	44.9	44.0
<sup>158</sup> Gd	2.8	0.18	10.6	0.50	0.348	65	63	12	6	10	0.08	3.29	3.28	23.5	23.5	14.9	15.1	20.4	20.3
<sup>156</sup> Dy	3.5	0.24	6.0	0.84	0.293	143	70	28	13	25	0.49	2.93	3.08	57.9	57.9	6.5	7.5	23.8	22.9
<sup>158</sup> Dy	2.4	0.24	7.7	0.58	0.326	54	78	28	8	20	0.46	3.21	3.21	75.4	74.8	9.6	10.3	19.1	18.2
<sup>160</sup> Dy	3.0	0.23	9.3	0.69	0.339	78	78	24	23	33	0.88	3.27	3.23	65.1	66.5	11.1	12.5	68.2	69.4
<sup>160</sup> Er	3.0	0.24	5.6	0.72	0.304	97	73	26	5	16	0.52	3.10	3.11	55.9	55.4	6.8	7.3	10.5	10.0
<sup>162</sup> Er	1.9	0.24	7.4	0.46	0.322	35	77	20	12	20	0.89	3.23	3.22	43.7	45.4	8.8	10.1	28.5	27.0
<sup>164</sup> Er	2.1	0.21	6.9	0.44	0.333	40	70	22	16	25	0.61	3.28	3.25	61.8	62.8	9.4	9.8	41.6	43.1
<sup>162</sup> Yb	2.4	0.25	4.0	0.60	0.263	83	66	24	4	14	0.33	2.92	3.05	39.9	39.1	4.8	5.3	7.1	6.9
<sup>164</sup> Yb	2.9	0.23	5.6	0.67	0.290	100	67	18	5	12	0.30	3.13	3.14	35.6	35.6	7.0	7.5	10.9	10.3
<sup>166</sup> Yb	2.4	0.23	7.0	0.55	0.315	58	72	24	13	23	0.82	3.23	3.22	62.3	63.9	9.1	9.6	31.2	30.0
<sup>168</sup> Yb	3.4	0.22	8.7	0.75	0.322	111	71	34	7	22	0.64	3.27	3.22	120.5	119.7	11.2	11.6	18.5	17.9
<sup>170</sup> Yb	2.6	0.22	10.1	0.57	0.326	64	72	20	14	22	0.63	3.29	3.26	52.7	54.1	13.6	14.0	39.3	39.9
<sup>172</sup> Yb	2.2	0.19	13.1	0.42	0.330	44	63	14	5	10	0.11	3.31	3.30	32.0	32.1	18.6	18.8	22.6	22.4
<sup>174</sup> Yb	2.6	0.20	15.1	0.52	0.325	64	65	18	5	12	0.13	3.31	3.30	50.2	50.4	21.4	21.5	25.2	25.0
<sup>176</sup> Yb	1.8	0.20	10.7	0.36	0.305	35	61	18	5	12	0.29	3.31	3.29	48.4	49.0	15.4	15.3	19.0	18.9
<sup>166</sup> Hf	2.2	0.25	4.1	0.55	0.250	77	63	22	3	12	0.24	2.97	3.08	36.9	36.5	5.1	5.5	6.3	6.2
<sup>168</sup> Hf	2.5	0.24	5.7	0.60	0.275	83	66	22	4	13	0.28	3.11	3.16	46.5	46.9	7.1	7.7	9.8	9.4
<sup>170</sup> Hf	3.9	0.22	7.9	0.86	0.301	168	66	34	4	19	0.48	3.19	3.16	105.7	105.3	9.5	10.1	12.2	11.7
<sup>172</sup> Hf	3.4	0.23	9.0	0.78	0.276	152	63	38	6	23	0.69	3.25	3.21	132.8	133.5	11.3	11.9	17.0	16.3
<sup>174</sup> Hf	3.1	0.23	10.2	0.71	0.286	117	66	22	4	13	0.43	3.27	3.24	58.2	58.9	13.5	13.7	15.9	15.5
<sup>176</sup> Hf	2.9	0.22	11.4	0.64	0.295	96	65	18	6	13	0.34	3.28	3.27	45.4	45.7	15.2	15.7	21.1	20.6
<sup>178</sup> Hf	2.2	0.22	9.2	0.48	0.280	62	62	18	6	13	0.41	3.29	3.26	44.2	45.0	12.6	12.9	18.1	17.8
<sup>176</sup> W	2.4	0.24	7.6	0.58				22	5	14	0.31	3.22	3.21	51.8	51.8	9.6	10.2	14.0	13.2
<sup>178</sup> W	2.4	0.23	7.6	0.55				14	2	7	0.14	3.24	3.23	27.0	27.2	10.5	10.4	10.5	10.4
<sup>180</sup> W	2.7	0.24	8.7	0.65	0.254	113	61	24	7	17	0.67	3.26	3.22	60.0	60.4	10.8	11.6	18.7	17.6
<sup>176</sup> Os	4.0	0.23	6.0	0.92				24	5	15	0.37	2.93	3.04	45.5	45.5	6.4	7.3	10.4	9.6
<sup>178</sup> Os	3.8	0.23	6.0	0.87				16	5	11	0.40	3.02	3.06	26.1	26.0	6.6	7.4	10.8	9.9
<sup>180</sup> Os	2.5	0.25	5.9	0.63	0.226	122	57	14	7	12	0.59	3.09	3.14	21.8	22.0	6.6	7.7	14.2	13.0
<sup>182</sup> Os	3.7	0.24	6.7	0.89	0.234	250	56	26	7	18	0.84	3.15	3.10	54.0	53.3	7.0	8.3	14.6	13.4
<sup>184</sup> Os	2.2	0.24	6.2	0.53	0.213	107	51	22	6	15	1.05	3.20	3.19	47.9	49.4	7.9	8.4	13.5	12.8
<sup>228</sup> Ra	3.1	0.24	10.1	0.74	0.217	204	52	22	3	12	0.18	3.21	3.23	53.6	54.0	13.3	13.3	14.1	14.0
<sup>228</sup> Th	3.5	0.24	13.1	0.84	0.230	231	55	18	5	12	0.15	3.24	3.25	41.7	41.6	16.8	17.1	20.3	20.0
<sup>230</sup> Th	2.8	0.22	10.6	0.62	0.244	132	54	18	4	11	0.12	3.27	3.26	45.1	45.3	14.7	14.7	16.6	16.6
<sup>232</sup> Th	2.4	0.23	12.1	0.55	0.261	85	60	30	12	25	0.54	3.28	3.27	104.6	105.9	15.9	16.6	36.5	35.6
<sup>232</sup> U	3.0	0.22	13.3	0.66	0.264	129	58	20	4	12	0.20	3.29	3.28	55.9	56.3	18.2	18.4	20.4	20.3
<sup>234</sup> U	2.7	0.23	15.9	0.62	0.272	99	63	28	7	19	0.36	3.30	3.29	98.8	99.6	21.3	21.8	29.0	28.5
<sup>236</sup> U	3.3	0.22	15.5	0.73	0.282	137	62	26	5	16	0.63	3.30	3.29	89.3	90.6	21.2	21.4	24.9	24.7
<sup>238</sup> U	2.9	0.23	18.3	0.67	0.286	103	66	30	27	40	0.85	3.30	3.29	112.1	114.9	23.6	25.0	112.7	113.5
<sup>240</sup> Pu	2.2	0.22	19.0	0.48	0.289	58	64	26	4	15	0.21	3.31	3.30	95.5	96.0	26.6	26.6	28.8	28.6
<sup>242</sup> Pu	2.3	0.22	17.7	0.51	0.292	62	64	26	2	13	0.51	3.31	3.30	93.7	94.8	24.7	24.8	24.7	24.8
<sup>248</sup> Cm	2.7	0.22	17.2	0.59	0.297	83	65	28	2	14	0.87	3.31	3.30	10.5	10.7	24.2	24.0	24.2	24.0

**Table 3.** Spectra of some rare earths and actinides, obtained with the parameters shown in Table 2.

$L$	$^{156}\text{Gd}$	$^{156}\text{Gd}$	$^{164}\text{Er}$	$^{164}\text{Er}$	$^{170}\text{Yb}$	$^{170}\text{Yb}$	$^{232}\text{Th}$	$^{232}\text{Th}$
	exp	th	exp	th	exp	th	exp	th
gsb								
4	3.24	3.25	3.28	3.25	3.29	3.26	3.28	3.27
6	6.57	6.59	6.72	6.60	6.80	6.66	6.75	6.69
8	10.85	10.86	11.21	10.92	11.43	11.07	11.28	11.13
10	15.92	15.88	16.61	16.11	17.06	16.37	16.75	16.47
12	21.63	21.56	22.79	22.09	23.54	22.49	23.03	22.60
14	27.83	27.78	29.58	28.83	30.63	29.36	30.04	29.45
16	34.39	34.50	37.33	36.29	37.92	36.94	37.65	36.97
18	41.29	41.66	45.10	44.44	45.18	45.21	45.84	45.11
20	48.62	49.23	53.28	53.27	52.66	54.13	54.52	53.85
22	56.49	57.18	61.85	62.77			63.69	63.16
24	64.95	65.49					73.32	73.03
26	73.99	74.15					83.38	83.45
28							93.82	94.39
30							104.56	105.86
$\gamma_1$								
2	12.97	14.49	9.41	9.80	13.60	14.02	15.91	16.59
3	14.03	15.27	10.36	10.65	14.54	14.85	16.80	17.41
4	15.24	16.29	11.58	11.77	15.78	15.95	18.03	18.49
5	16.94	17.55	13.10	13.15	17.33	17.31	19.45	19.82
6	18.47	19.04	14.87	14.78	19.01	18.92	21.27	21.41
7	20.79	20.74	16.91	16.65	21.13	20.78	23.21	23.23
8	22.61	22.65	19.09	18.76	23.19	22.87	25.50	25.29
9	25.29	24.74	21.64	21.08	25.76	25.18	27.75	27.57
10	27.45	27.02	23.90	23.63	28.16	27.72	30.62	30.06
11	30.20	29.47	27.13	26.38	30.90	30.47	33.22	32.75
12	32.85	32.08	29.91	29.33	33.55	33.42	36.48	35.64
13	35.69	34.84	33.13	32.48	36.40	36.57		
14	38.64	37.74	35.75	35.83	39.25	39.91		
15	41.76	40.78	38.51	39.36				
16	44.90	43.95	41.59	43.07				

**Table 4.** Same as Table 2, for 17 additional nuclei. See subsection 5.1 for further discussion.

nucleus	$\tilde{\beta}_0$	$\tilde{A}$	$C$	$\tilde{a}_0$	$\beta_0$	$V_0$	$10^3 a_0$	$L_g$	$L_\gamma$	$N$	$\sigma$	4/2 exp	4/2 th	$L_g/2$ exp	$L_g/2$ th	$2_\gamma/2$ exp	$2_\gamma/2$ th	$L_\gamma/2$ exp	$L_\gamma/2$ th
<sup>160</sup> Gd	1.8	0.18	9.0	0.32	0.353	26	64	16	8	14	0.10	3.30	3.29	40.0	40.2	13.1	13.1	22.8	22.8
<sup>162</sup> Gd	1.5	0.18	8.2	0.27				14	4	9	0.05	3.29	3.29	31.4	31.5	12.0	12.0	14.1	14.1
<sup>162</sup> Dy	1.9	0.19	7.7	0.36	0.343	31	65	18	14	21	0.23	3.29	3.28	47.6	47.9	11.0	11.1	39.4	39.2
<sup>164</sup> Dy	1.2	0.19	7.1	0.23	0.348	12	66	20	10	18	0.26	3.30	3.28	57.4	58.1	10.4	10.4	25.3	25.3
<sup>166</sup> Dy	1.2	0.15	7.5	0.18				6	5	6	0.02	3.31	3.30	6.9	6.8	11.2	11.2	14.9	14.9
<sup>166</sup> Er	1.2	0.21	6.9	0.25	0.342	12	72	16	14	20	0.30	3.29	3.26	36.8	37.1	9.8	9.9	35.7	36.6
<sup>168</sup> Er	1.2	0.16	6.9	0.19	0.338	13	54	18	8	15	0.20	3.31	3.30	50.0	50.6	10.3	10.3	20.4	20.3
<sup>170</sup> Er	0.7	0.18	8.9	0.13	0.336	4	61	26	19	30	0.85	3.31	3.30	95.8	98.1	11.9	13.0	66.2	65.7
<sup>178</sup> Yb	1.3	0.17	9.9	0.22				6	2	3	0.01	3.31	3.30	6.9	6.9	14.5	14.5	14.5	14.5
<sup>180</sup> Hf	1.0	0.16	8.7	0.16	0.274	13	44	12	5	9	0.05	3.31	3.30	24.3	24.4	12.9	12.9	16.7	16.6
<sup>182</sup> W	1.4	0.20	8.6	0.28	0.251	31	50	18	6	13	0.26	3.29	3.28	47.4	48.0	12.2	12.4	17.7	17.6
<sup>184</sup> W	0.9	0.18	5.4	0.16	0.236	15	43	10	6	9	0.06	3.27	3.28	16.7	16.8	8.1	8.0	13.3	13.4
<sup>186</sup> W	1.0	0.19	4.1	0.19	0.226	20	43	14	6	11	0.09	3.23	3.25	29.1	29.2	6.0	6.1	11.4	11.4
<sup>186</sup> Os	1.7	0.22	4.2	0.37	0.200	72	44	14	13	18	0.20	3.17	3.19	25.9	26.1	5.6	6.1	26.5	26.8
<sup>188</sup> Os	1.4	0.23	3.0	0.32	0.186	57	43	12	7	11	0.18	3.08	3.14	18.4	18.7	4.1	4.4	10.9	10.6
<sup>190</sup> Os	1.4	0.24	2.2	0.34	0.178	62	43	10	6	9	0.20	2.93	3.06	12.6	12.7	3.0	3.3	7.9	7.6
<sup>238</sup> Pu	1.7	0.21	16.5	0.36	0.286	35	60	26	4	15	0.34	3.31	3.30	96.8	97.6	23.3	23.4	25.5	25.5

**Table 5.** Comparison of theoretical predictions of the Bohr Hamiltonian with the Woods–Saxon potential to experimental data [21] for 9  $\gamma$ -unstable Xe isotopes with  $R_{4/2} < 2.6$  and known  $0_2^+$  and  $2_\gamma^+$  states. The angular momenta of the highest levels of the ground state and quasi- $\gamma_1$  bands included in the rms fit are labelled by  $L_g$  and  $L_\gamma$  respectively, while  $N$  indicates the total number of levels involved in the fit and  $\sigma$  is the quality measure of (66). All energies are normalized to the energy of the first excited state,  $E(2_1^+)$ . For each band, the  $R_{4/2} = E(4_1^+)/E(2_1^+)$  ratio (labelled by 4/2), the normalized bandhead of the quasi- $\gamma_1$  band (labelled as  $2_\gamma/2$ ), and the normalized last members of the ground state and quasi- $\gamma_1$  bands included in the fit (labelled by  $L_g/2$  and  $L_\gamma/2$  respectively), are reported.  $\beta_0$  has been obtained from [71]. The theoretical predictions are obtained from (44). See subsection 5.2 for further discussion.

nucleus	$\tilde{\beta}_0$	$\tilde{A}$	$10^3 \tilde{a}_0$	$\beta_0$	$V_0$	$10^3 a_0$	$L_g$	$L_\gamma$	$N$	$\sigma$	4/2 exp	4/2 th	$L_g/2$ exp	$L_g/2$ th	$2_\gamma/2$ exp	$2_\gamma/2$ th	$L_\gamma/2$ exp	$L_\gamma/2$ th
<sup>118</sup> Xe	0.13	0.18	23	0.265	0.2	48	14	8	13	0.26	2.40	2.34	12.9	13.1	2.8	2.3	7.8	8.0
<sup>120</sup> Xe	0.21	0.17	36	0.291	0.5	50	14	9	14	0.47	2.47	2.37	13.8	13.6	2.7	2.4	9.8	10.8
<sup>122</sup> Xe	0.52	0.14	71	0.259	4.0	35	16	9	15	0.65	2.50	2.32	17.5	17.6	2.5	2.3	9.7	11.1
<sup>124</sup> Xe	0.57	0.16	88	0.212	7.2	33	12	8	12	0.51	2.48	2.32	11.0	10.8	2.4	2.3	8.2	8.2
<sup>126</sup> Xe	0.65	0.18	115	0.188	11.9	33	12	9	13	0.63	2.42	2.28	11.0	10.1	2.3	2.3	9.1	10.1
<sup>128</sup> Xe	0.67	0.21	143	0.184	13.4	39	10	7	10	0.47	2.33	2.20	7.6	6.9	2.2	2.2	6.2	6.9
<sup>130</sup> Xe	0.92	0.22	203	0.169	29.4	37	14	5	10	0.30	2.25	2.11	9.5	9.5	2.1	2.1	4.1	4.7
<sup>132</sup> Xe	0.90	0.24	218	0.141	41.2	34	6	2	3	0.34	2.16	2.05	3.2	3.2	1.9	2.1	1.9	2.1
<sup>134</sup> Xe	1.10	0.27	302	0.119	85.6	33	8	5	7	0.29	2.04	1.82	3.5	3.1	1.9	1.8	2.7	3.1